International Journal of Nanomedicine

Dovepress

open access to scientific and medical research

Open Access Full Text Article

ORIGINAL RESEARCH

Novel Nanohydroxyapatite (nHAp)-Based Scaffold Doped with Iron Oxide Nanoparticles (IO), Functionalized with Small Non-Coding RNA (miR-21/124) Modulates Expression of Runt-Related Transcriptional Factor 2 and Osteopontin, Promoting Regeneration of Osteoporotic Bone in Bilateral Cranial Defects in a Senescence-Accelerated Mouse Model (SAM/P6). PART 2

Krzysztof Marycz,[1,2] Agnieszka Śmieszek,[1] Katarzyna Kornicka-Garbowska,[1,2] Ariadna Pielok,[1] Maciej Janeczek,[3] Anna Lipińska,[3] Anna Nikodem,[4] Jarosław Filipiak,[4] Paulina Sobierajska,[5] Jean-Marie Nedelec,[6] Rafał J Wiglusz[2,5]

[1]Department of Experimental Biology, Wroclaw University of Environmental and Life Sciences, Wroclaw, 50-375, Poland; [2]International Institute of Translational Medicine, Malin, 55-124, Poland; [3]Department of Biostructure and Animal Physiology, Wroclaw University of and Life Sciences, Wroclaw, 51-631, Poland; [4]Department of Mechanics, Materials and Biomedical Engineering, Wroclaw University of Science and Technology, Wybrzeze Wyspianskiego 27, 50-370 Wrocław, Poland; [5]Institute of Low Temperature and Structure Research, Polish Academy of Sciences, Okolna 2, 50-422 Wroclaw, Poland; [6]Universite Clermont Auvergne, Clermont Auvergne INP, CNRS, ICCF, Clermont-Ferrand, France

Correspondence: Krzysztof Marycz
The Department of Experimental Biology, The Faculty of Biology and Animal Science, University of Environmental and Life Sciences Wroclaw, Norwida 27B St, Wroclaw, 50–375, Poland
Tel +48 71 320 5201
Email krzysztof.marycz@upwr.edu.pl

Purpose: Healing of osteoporotic defects is challenging and requires innovative approaches to elicit molecular mechanisms promoting osteoblasts-osteoclasts coupling and bone homeostasis.

Methods: Cytocompatibility and biocompatibility of previously characterised nanocomposites, i.e $Ca_5(PO_4)_3OH/Fe_3O_4$ (later called nHAp/IO) functionalised with microRNAs (nHAp/IO@miR-21/124) was tested. In vitro studies were performed using a direct co-culture system of MC3T3-E1 pre-osteoblast and 4B12 pre-osteoclasts. The analysis included determination of nanocomposite influence on cultures morphology (confocal imaging), viability and metabolic activity (Alamar Blue assay). Pro-osteogenic signals were identified at mRNA, miRNA and protein level with RT-qPCR, Western blotting and immunocytochemistry. Biocompatibility of biomaterials was tested using bilateral cranial defect performed on a senescence-accelerated mouse model, ie SAM/P6 and Balb/c. The effect of biomaterial on the process of bone healing was monitored using microcomputed tomography.

Results: The nanocomposites promoted survival and metabolism of bone cells, as well as enhanced functional differentiation of pre-osteoblasts MC3T3-E1 in co-cultures with pre-osteoclasts. Differentiation of MC3T3-E1 driven by nHAp/IO@miR-21/124 nanocomposite was manifested by improved extracellular matrix differentiation and up-regulation of pro-osteogenic transcripts, ie late osteogenesis markers. The nanocomposite triggered bone healing in a cranial defect model in SAM/P6 mice and was replaced by functional bone in Balb/c mice.

Conclusion: This study demonstrates that the novel nanocomposite nHAp/IO can serve as a platform for therapeutic miRNA delivery. Obtained nanocomposite elicit pro-osteogenic signals, decreasing osteoclasts differentiation, simultaneously improving osteoblasts metabolism and their transition toward pre-osteocytes and bone mineralisation. The proposed scaffold can be an effective interface for in situ regeneration of osteoporotic bone, especially in elderly patients.

Keywords: senile osteoporosis, osteoblasts, osteoclasts, nanohydroxyapatite, iron oxide nanoparticles, small non-coding RNA

Received: 21 April 2021
Accepted: 28 July 2021
Published: 31 August 2021

Introduction

The prevalence of osteoporosis (OP) is rapidly increasing, especially in well-developed countries. The ageing of society and longer life expectancy enhance the economic burden of disease and challenge health care systems.[1] The major clinical characteristics of OP include decreased bone mass and micro-architectural deterioration of the tissue. Due to impaired bone structure, an increased risk of fragility fracture, is a characteristic, especially in elderly people. Worldwide, OP each year contributes to >8.9 million fractures, of which most occur in Europe.[1,2]

The advancement in the field of osteoporosis treatment and prevention is undeniable, however, bone fracture regeneration in osteoporotic/geriatric patients is still problematic, hence requires novel therapeutic strategies.[3–5]

At the molecular level, the disease is triggered by an imbalance between the activity of bone-forming and resorbing cells.[6,7] In bone formation, mesenchymal stromal stem cells (MSCs), which can differentiate into pre-osteoblast populations and play a fundamental role in initiating tissue regeneration, represent one of the most promising therapeutic targets.[8–10] In turn, in the case of bone resorption, the crucial role is played by the activity of osteoclasts, which absorb fully mineralised bone.[11] Thus, targeting these cells cytophysiological features may become a novel therapeutic strategy during bone fracture healing.[12]

One of the approaches to enhance healing of OP fractions is the fabrication of novel, personalised biomaterials, and thus far, various scaffolds and drug delivery systems have been developed, yet most of them lack the bioactivity and pleotropic effects to inhibit disease progression at the cellular level.[13–15] For this reason, the major goal of the presented study was to fabricate a novel scaffold that not only mechanically supports bone regeneration but also restores the physiological balance between osteoblasts and osteoclasts via targeted and controlled delivery of bioactive molecules into recipient cells. Due to its unique characteristics, including bioactivity, biocompatibility, stability, nontoxic properties, and the presence of –OH groups, which can be employed to conjugate drugs or other chemicals, nanohydroxyapatite (nHAp) has been frequently applied in the fabrication of synthetic bone grafts and bone cements.[16,17] What is more, due to its chemical properties, nHAp can be modified with different molecules, which enable the fabrication of platforms with the capability of controlled release. Conjugation with Fe_3O_4, iron oxide nanoparticles (IO) creates a molecular bridge between nHAp and the selected molecules released into the injury sites. The application of an external static magnetic field (SMF) breaks the bonding between the composite and causes its discharge.[18] Interestingly, IO are non-toxic, biocompatible, and bioactive, which supports their application in the fabrication of smart (bio-intelligent) materials. In our previous studies, we have shown that IO modulate the metabolic activity of osteoblasts and osteoclasts and do not elicit an immune response. In search of new bioactive and therapeutic molecules that can be utilised in the treatment of selected disorders, miRNAs are one of the most potent and attractive. MiRNAs belong to non-coding RNAs that function as a post-transcriptional repressor by binding to complementary sites on the target mRNA. These small molecules play a crucial role in multiple cellular processes, including differentiation, proliferation, and apoptosis.[7,19] Recently, miRNAs have been shown to also participate in bone regeneration by affecting MSC and osteoclast fate. For the fabrication of the material presented in this paper, miR-21 and miR-124 were selected to control osteoblast and osteoclast activity, respectively. It was shown that overexpression of miR-21 by MSCs increased the expression of osteopontin and alkaline phosphatase but also promoted mineralisation in the condition of osteogenic induction.[20,21] Moreover, the bone healing properties were enhanced in the fracture healing model according to the results of micro-CT, mechanical test, and histological analysis. On the other hand, miR-124, a specific suppressor of NFATc1, can diminish osteoclast differentiation, proliferation, and migration.[22,23] Thus, combining these two miRNAs as a therapeutic approach in osteoporotic bone regeneration is fully justified.

In the following study, we tested a novel biomaterial with controlled delivery of bioactive agents for osteoporotic bone fracture regeneration. The presented scaffold is composed of the nHAp, which supports the formation of a new matrix and stands as a material core. In turn, selected miRNAs enhance the activity of osteoblasts and diminish the activity of osteoclasts, which contributes to the functional regeneration of osteoporotic bone. The effectiveness of the fabricated materials has been tested in the presented studies in vitro using a co-culture model of MC3T3-E1 and 4B12 cell lines and in vivo with a senescence-accelerated mouse (SAM/P6) model reflecting the reduction of bone mass and its biomechanics, which occurs in elderly, osteoporotic patients.

Materials and Methods

Cell Culture

The murine osteoblast precursor cell line (MC3T3-E1) was provided by the European Collection of Authenticated Cell Cultures (ECACC, Sigma Aldrich, Munich, Germany). Cells were maintained in a complete growth medium ($CGM_{MC3T3-E1}$) consisting of Minimum Essential Media Alpha without ascorbic acid (MEM-α, Gibco, Scotland, UK) with the addition of 10% Fetal Bovine Serum (FBS, Sigma-Aldrich, Munich, Germany). Pre-osteoclastic murine cell line (4B12) was kindly provided by Professor Shigeru Amano (Department of Oral Biology and Tissue Engineering, Meikai University School of Dentistry in Japan). Complete culture medium for 4B12 cells (CGM_{4B12}) consisted of Minimum Essential Medium Eagle, Alpha Modification (MEM-α, Sigma Aldrich, Munich, Germany) supplemented 10% of FBS and 30% of calvaria-derived stromal cell-conditioned medium (CSCM).[24] The cells were cultured at constant conditions in CO_2 incubator at 37°C, 5% CO_2 and 95% humidity. The culture media were changed every 2–3 days. Subculturing of cells was performed when the confluence of the cells in the culture dish reached 80%. Detailed protocols for trypsinisation of pre-osteoblasts and osteoclast precursors were established and published previously.[7,25,26]

Evaluation of nHAp/IO Cytocompatibility

Cell Culture

A direct co-culture model of pre-osteoblasts and pre-osteoclasts was used to test the cytocompatibility of the obtained biomaterials. The MC3T3-E1 cells were inoculated in 24-well plates at the density of 3×10^4 cells/well. After 12 h, ie when MC3T3-E1 adhered to the surface of the dish, the 4B12 preosteoclast were added to the culture at a density of 1×10^3 cells/well. The final volume of the growth medium was equal to 500 µL. In turn, osteogenic cultures were performed using 6-well plates. For this purpose, pre-osteoblastic MC3T3-E1 cells were inoculated at a density equal to 1.5×10^5 cells. Following pre-osteoblasts adhesion, the 4B12 cell line was inoculated at a density of 1.5×10^3 cells/well. The pro-osteogenic medium, ie MEM-α supplemented with osteogenic factors, including 10 nM β-glycerol phosphate disodium salt hydrate and 50 µg/mL ascorbic acid, was introduced after 24 hours of cells inoculation in a total volume of 2 mL.

Biomaterials were obtained using an established protocol, and their complete physicochemical characterisation was described previously.[27] In this study, the obtained nHAp/IO and nHAp/IO@miR-21/124 biomaterials were introduced to the co-cultures at a concentration of 10% of the complete growth medium. The cytocompatibility was tested without (MF-) and under magnetic field influence (MF+). Cultures exposed to the magnetic field (MF+) were incubated each day of culture for 15 min in a system provided by the Institute of Low Temperature and Structure Research Polish Academy of Sciences in Wroclaw and described in detail by Marycz et al.[18] The system installed in CO_2 incubator generated magnetic field (MF) strength was equal to 0.2 T. Experiment was carried out for 4 days to evaluate the cytotoxic effect, while osteogenesis was induced for 14 days, the media were replaced every 3 days.

Evaluation of Biomaterials Cytotoxicity

The potential cytotoxic effect of nHAP/IO and nHAP/IO@miR-21/124 was tested based on ultrastructural features of cells, and mitochondrial metabolism determined using Alamar Blue assay. The metabolic activity of cells measured with Alamar Blue assay was evaluated after 4 days of the experiment, using the protocol established previously and according to the manufacturer's instructions.[28] For confocal imaging, cultures were fixed with 4% paraformaldehyde (PFA) for 15 min at room temperature. The mitochondria network structure was determined after its staining with MitoRed dye (Sigma-Aldrich, Munich, Germany). Actin cytoskeleton was visualised using a solution of phalloidin-Atto 488 (Sigma-Aldrich, Munich, Germany) prepared at a concentration of 1:800 in phosphate-buffered saline pH 7.4. Mitochondria and cytoskeleton staining were described in detail elsewhere.[29] The specimens were preserved using Mounting Medium with DAPI ([4′,6-diamidino-2-phenylindole], Thermo Fisher Scientific, Waltham, MA, USA) for nuclei counterstain. The specimens imaging was done with confocal fluorescence microscopy (Leica TCS SPE, Leica Microsystems, Wetzlar, Germany) under 630× magnification. The analysis was also supported by measuring mRNA-coding anti- and pro-apoptotic molecules, Bcl-2 and Bax, respectively. The description of transcripts determination is described below.

Effectiveness of in vitro Osteogenesis in a Co-Culture System

The formation of calcium deposits in osteogenic cultures was determined after staining with Alizarin Red S dye (Sigma-Aldrich, Munich, Germany). The extracellular matrix (ECM) mineralisation was evaluated under an inverted microscope (Axio Observer A1; Zeiss, Oberkochen, Germany). The microphotographs of ECM, as well as images of osteogenic cultures, were captured using Canon PowerShot digital camera (Woodhatch, UK). Signals obtained after Alizarin staining were counted using ImageJ and Pixel Counter plugin (version 1.6.0, U. S. National Institutes of Health, Bethesda, MD, USA), also described in our previous publications.[7]

The effectiveness of osteogenesis in vitro was determined based on the expression of molecules involved in bone remodelling. Transcripts levels (mRNA and miRNA) were determined using RT-qPCR technique. Total RNA was isolated with phenol-chloroform method after homogenisation with Extrazol® (Blirt DNA, Gdańsk, Poland) accordingly to the manufacturer's protocol. The isolated RNA quality was determined using a microspectrophotometer (Epoch, BioTek Instruments, Vermont, USA). The residues of genomic DNA were removed from specimens using PrecisionDNAse Kit (Primerdesign, BLIRT S.A., Gdańsk, Poland). The reverse transcriptase (RT) reaction was performed using Tetro cDNA Synthesis Kit (Bioline Reagents Limited, London, UK) for mRNA detection and with Mir-X™ First-Strand Synthesis Kit (Takara Clontech Laboratories, Mountain View, CA, USA) for detection of miRNA levels. Quantitative PCR (qPCR) measurement was done using SensiFAST SYBR Green® & Fluorescein Kit (Bioline Reagents Ltd., London) on CFX Connect Real-Time PCR Detection System (Bio-Rad, Hercules, CA, USA). Each reaction was performed in triplicate. The details of the RT-qPCR protocols used were previously published.[7,30] Characteristics of primers used in qPCR are presented in Table 1. In order to determine the relative levels of tested transcripts, the RQ_{MAX} algorithm was used. Normalisation was performed to reference genes levels, ie glyceraldehyde 3-phosphate dehydrogenase (Gapdh) for mRNA levels and small nuclear RNA U6 (snU6) for targeted miRNA levels.

Protein levels were determined using the Western Blot technique. The reaction details were previously published.[7] Here, the protein concentration in each tested sample was equal to 20 µg. The primary antibodies used to detect runt-related transcription factors (anti-RUNX-2, cat. no sc-390351, Santa Cruz Biotechnology, Dallas, Texas, USA) and osteopontin (anti-OPN, cat no. ab8448, Abcam, Cambridge, UK) were diluted in the ratio 1:100 and 1:1000, respectively. Moreover, intracellular localisation of RUNX-2 and OPN was identified using immunocytochemistry technique and confocal fluorescence imaging. The complete methodology of the performed staining was described previously.[7] The secondary antibodies were anti-Mouse IgG-Atto 594 antibody produced in goat (cat. no 76085, Sigma-Aldrich, Munich, Germany) and anti-Rabbit IgG-Atto 594 antibody produced in goat (cat. no 77671, Sigma-Aldrich, Munich, Germany). The secondary antibodies were diluted at a concentration of 1:1000. The microscopic analyses were performed using a confocal microscope under 630× magnification (Leica TCS SPE, Leica Microsystems, Wetzlar, Germany). Furthermore, Colour Pixel Counter plugin within Fiji is New ImageJ software (version 1.52n, Wayne Rasband, National Institutes of Health, USA) was used to count the intensity of RUNX-2 and OPN accumulation. Each measurement was done in triplicate.

The Effectiveness of New Bone Formation Guided by the Biomaterial Presence – In vivo

The following study was performed with the full approval of the Local Ethics Committee for Animal Experiments in Wroclaw (Resolution no.069/2020, 9.12.2020). During the experiment, we followed guidelines included within the Act on the Protection of Animals Used for Scientific or Educational Purposes from 15 of January 2015, which implements Directive 2010/63/EU of the European Parliament and the Council of 22 September 2010. We used the procedures of PN-EN ISO 10993–2:2006 standards. All SAMP-6 mice used in this study were purchased from Envigo (Indianapolis, IN, United States), while the BALB/c mice were purchased from a local distributor (Mirosław Mossakowski Institute of Experimental and Clinical Medicine, Warsaw, Poland). The experiment was preceded by a one-week acclimatisation period. All animals were housed under a 12 h light/dark cycle with constant temperature (22±2°C) and humidity (50±10%). Mice were fed a standard chow diet and had access to water ad libitum. In the study, BALB/c mice (n=2) were used as a healthy control, while SAMP6 mice (n=2) represented an osteoporotic model. In order to assess the biocompatibility of the tested implants, a bilateral cranial

Table 1 The Characterisation of Primers Used for RT-qPCR Analyses

Gene	Primer Sequence 5′-3′	Annealing Temperature [°C]	Accesion No. of Sequence
Bcl-2	F: GGATCCAGGATAACGGAGGC	58.8	NM_000633.2
	R: ATGCACCCAGAGTGATGCAG		
Bax	F: AGGATGCGTCCACCAAGAAGC	58.8	NM_001291428.1
	R: GGTTCTGATCAGCTCGGGCA		
Runx-2	F:TCCGAAATGCCTCTGCTGTT	58.8	NM_001271630.1
	R:GCCACTTGGGGAGGATTTGT		
Opn	F: AGACCATGCAGAGAGCGAG	57.3	NM_001204203.1
	R: GCCCTTTCCGTTGTTGTCCT		
Sost	F: AGCCTTCAGGAATGATGCCAC	51.2	NM_024449.6
	R: CTTTGGCGTCATAGGGATGG		
Dmp1	F: CCCAGAGGCACAGGCAAATA	60.0	NM_001359013.1
	R: TCCTCCCCAATGTCCTTCTT		
Ocn	F: CTCCTGAGAGTCTGACAAAGCCTT	58.8	NM_007541.3
	R: GCTGTGACATCCATTACTTGC		
Alp	F: AACGTGGCCAAGAACATCATCA	58.8	NM_007431.3
	R: TGTCCATCTCCAGCCGTGTC		
Coll-1	F:CAGGGTATTGCTGGACAACGTG	61.4	NM_007742.4
	R:GGACCTTGTTTGCCAGGTTCA		
Ctsk	F: TAACAGCAAGGTGGATGAAATCT	60.0	NM_011613.3
	R: CTGTAGGATCGAGAGGGAGGTAT		
Trap	F: GTCTCTGGGGGACAATTTCTACT	58.8	XM_006509945.3
	R: GTTTGTACGTGGAATTTTGAAGC		
Gapdh	F: TGCACCACCAACTGCTTAG	58.8	XM_017321385.2
	R: GGATGCAGGGATGATGTTC		
miR-7a-5p	TGGAAGACTAGTGATTTTGTTGT	58.8	MIMAT0000677
miR-17-5p	CAAAGTGCTTACAGTGCAGGTAG	58.8	MIMAT0000649
miR-21-5p	TAGCTTATCAGACTGATGTTGA	58.8	MIMAT0000530
miR-124-3p	TAAGGCACGCGGTGAATGCC	58.8	MIMAT0000134
miR-223-3p	TGTCAGTTTGTCAAATACCCCA	58.8	MIMAT0000280
miR-320-3p	AAAAGCTGGGTTGAGAGGGCGA	58.8	MI0000704

Abbreviations: nHAp, nanohydroxyapatite; IOs, iron oxide nanoparticles; miR, microRNA; RT-qPCR, quantitative polymerase chain reaction followed by reverse transcription; XRPD, X-ray powder diffraction; MF, magnetic field; Runx-2, runt-related transcription factor 2; Coll-1, collagen type 1; OPG, osteoprotegerin; Bcl-2, B-cell lymphoma 2; BAX, Bcl-2 associated X protein; Sost, sclerostin; Dmp1, dentin matrix protein 1; TRAP, tartrate-resistant acid phosphatase; OPN, osteopontin; ALP, alkaline phosphatase; CAII, anhydrase II; Ctsk, cathepsin K; Gapdh, glyceraldehyde 3-phosphate dehydrogenase; snU6, small nuclear; RNA OCN, osteonectin; ECM, extracellular matrix; DAPI, [4′,6-diamidino-2-phenylindole].

defect model was performed. Details of the procedure were described elsewhere.[31] The implant was placed at the right defect site, while the left defect site was left empty as a control. Subsequently, mice were euthanized 6 weeks after the cranial defect procedure to assess novel bone tissue formation.

For the microCT analyses, mice skulls were dissected, and all remaining soft tissue was carefully removed without disturbing the sample. The measurements were performed using Skyscan 1172 microCT system (Bruker, Kontich, Belgium). Each sample was recorded with a 3.2 µm resolution and the following lamp parameters 73kV/135uA with an additional 0.5 mm Al filter. The exposure time was 1617 ms, the total rotation angle of the tripod was 180°, and the unit rotation angle was 0.2°. Measurements of 3D structural properties were carried out with the use of DataViewer and CTAn programs. In order to determine the influence of implants on the structure of the newly formed bone tissue, the following stages of research were carried out: qualitative research on the bone tissue in the peri-implantation area, measurement of the diameters of the cranial defects and analysis of the structural properties of peri-implant bone tissue. 2D examination was performed with the use of CTAn software in order to assess the diameter of cranial defects. For each defect, a 2 mm area was measured, as this was the size of the initial cranial defect. The assessed parameters include defect circularity and geometry aspect ratio, which depend on the defect diameter differences and the volume content of the newly formed bone tissue in the measured area (BV/TV). The peri-implantation tissue area was selected as the 3 mm diameter surface around the implantation site (without new bone tissue).

Statistical Analysis

Results obtained during in vitro and in vivo studies were presented as the mean with standard deviation (±SD), derived from at least three technical repetitions of the detailed analysis. The statistical calculations were made with parametric assays: t-Student test or One-way analysis of variance with Dunnett's post hoc test. GraphPad Software (Prism 8.20, San Diego, CA, USA) was used for testing and graphical data presentation. Prior to the analysis, the normality of the population data was evaluated with Shapiro–Wilk test. In turn, the equality of variances was assessed by Levene's test (STATISTICA 10.0 software, StatSoft, Inc., Statistica for Windows, Tulsa, OK, USA. In the comparative analysis, differences described with a probability of $p < 0.05$ were considered significant.

Results

The Influence of the Scaffold on Morphology and Viability of MC3T3-E1/4B12 Co-Cultures

The evaluation of cytocompatibility of the nanocomposites was determined without and under the influence of magnetic field (MF- and MF+, respectively). The microscopic observation revealed that obtained biomaterials do not alter the growth pattern of MC3T3-E1/4B12 co-cultures. The predominance of osteoblast progenitors, with a characteristic fibroblastic-like phenotype, was evident. The cells had a rounded, centrally located nucleus and well-developed mitochondrial network, as well as actin cytoskeleton (Figure 1A). The analysis of cells viability based on transcript levels for anti-apoptotic Bcl-2 and pro-apoptotic Bax indicated pro-survival activity of tested nanocomposites (Figure 1B–D). The functionalisation of nHAp/IO matrices with miRNA complex did not affect the Bax/Bcl-2 ratio (Figure 1D).

The nHAp/IO@miR-21/124 Modulates the Metabolic Activity of MC3T3-E1/4B12 Co-Cultures

The metabolic activity determined based on mitochondrial enzymes activity was modulated by the nanocomposites and the magnetic field. Significantly increased metabolism was noted in MC3T3-E1/4B12 co-cultures with nHAp/IO@miR-21/124. Magnetic field promoted the metabolic activity of cells. However, the modulatory effect of nanocomposites in cultures stimulated by the magnetic field was not observed (Figure 1E).

The Increased Osteogenesis and Extracellular Matrix (ECM) Mineralisation Supported by the Scaffold

Analysis of the pro-osteogenic action of nanocomposites showed improved extracellular matrix (ECM) mineralisation guided by the presence of biomaterial (Figure 2A and B). Moreover, increased deposition of calcium was noted in cultures exposed to the magnetic field. The most potent pro-osteogenic effect resulted from cells propagation with nanocomposite functionalised with miRNA complex. The biomaterial enhanced mineralisation of ECM regardless of the magnetic field influence (Figure 2B).

Modulatory Effect of the Scaffold on Bone-Related Transcripts (mRNA Level)

The expression profile of transcripts associated with bone remodelling, determined for cultures propagated with nanocomposites, showed pattern characteristic for functional and mineralised bone tissue (Figure 3). In MC3T3-E1/4B12 cultures propagated with the addition of nHAp/IO, both alone and functionalised with miR-21/124, we have observed

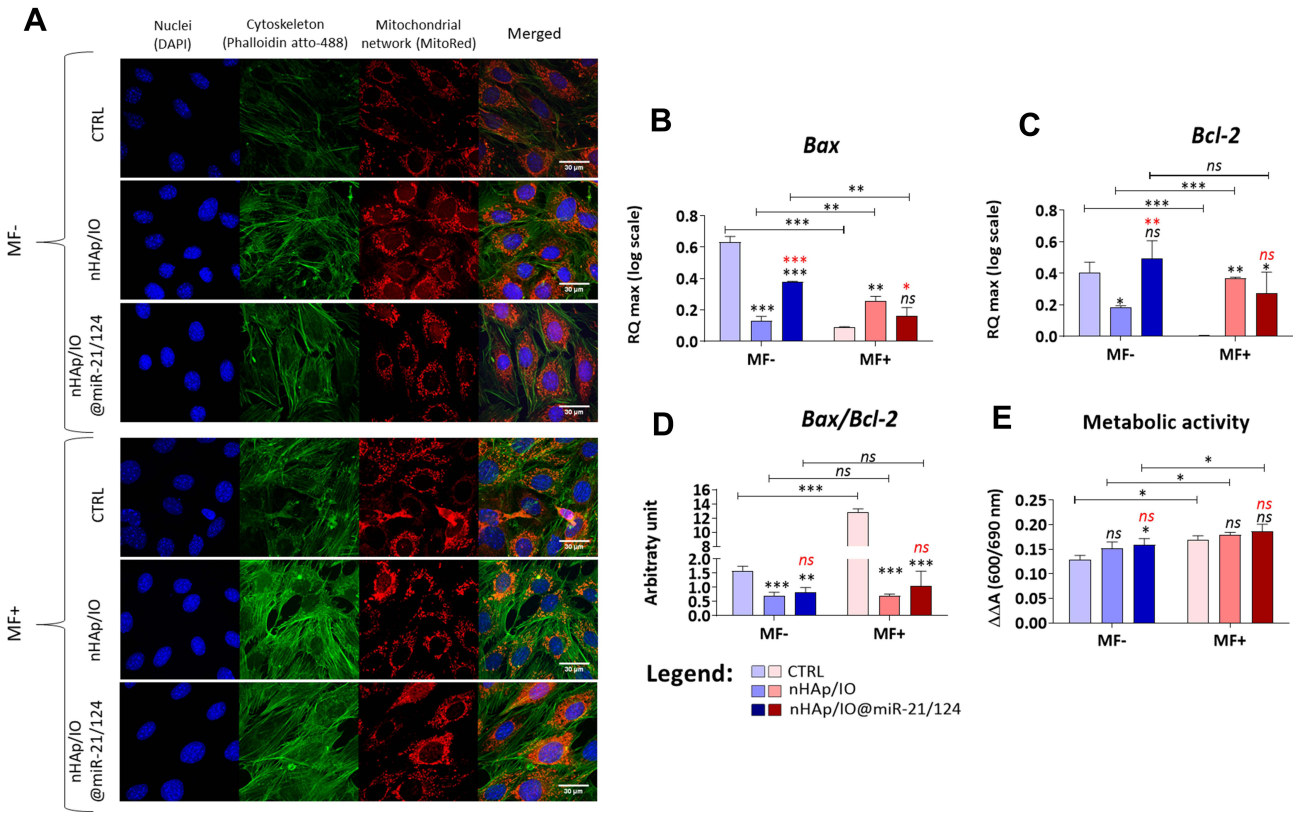

Figure 1 Obtained nanocomposites are cytocompatible and promote survival and metabolism of MC3T3-E1/4B12 co-cultures. (**A**) Confocal imaging of the cultures growth pattern and ultrastructure propagated without and under magnetic field influence. Scale bar = 30 μm. (**B**) The transcript levels for Bax determined with RT-qPCR technique. (**C**) Measurement of mRNA expression for Bcl-2. (**D**) The relative Bax/Bcl-2 ratio. (**E**) Metabolism of cells determined based on mitochondrial enzymes activity. Obtained data were used for comparative analysis and presented as columns with bars representing means ± SD. Marks: *p<0.05; **p < 0.01; ***p<0.001 and non-significant differences were indicated using ns symbol. The differences between nHAp/IO and nHAp/IO@miR-21/124 were marked with red font.

increased mRNA expression for sclerostin (*Sost;* Figure 3A) and dentin matrix protein 1 (*Dmp1;* Figure 3B). Simultaneous accumulation of transcripts for Sost and Dmp1 is characteristic for late osteoblasts/preosteocytes, as well as osteocyte-like cells differentiating in vitro. Concomitantly, in cultures with biomaterials, we have observed enhanced expression of transcripts associated with late osteogenesis, including osteocalcin (*Ocn;* Figure 3D) and collagen type 1 (*Coll-1;* Figure 3E) and decreased expression of alkaline phosphate (*Alp;* Figure 3C) activated at the early stages of osteoblast differentiation. The expression profile corresponds to fully developed and mineralised ECM in vitro, observed in cultures with biomaterials. Simultaneously, the increased mRNA levels for cathepsin K (*Ctsk;* Figure 3F) and lowered mRNA levels for tartrate-resistant acid phosphatase (*Trap;* Figure 3G) were characteristic of MC3T3-E1/4B12 co-cultures propagated with obtained nanocomposites. The magnetic field exposition also modulated the expression of pro-osteogenic transcripts, increasing accumulation of *Sost* and *Dmp1* in cultures with nHAp/IO, as well as *Ocn* in cultures treated with nHAp/IO@miR-21/124. The magnetic field exposure was also associated with decreased mRNA levels for *Trap*, noted in cultures with nanomaterials (Figure 3G). Furthermore, we observed that the expression of RUNX2 was elevated in MC3T3-E1/4B12 cells cultured with nHAp/IO@miR-21/124 nanocomposite when compared to the control. Interestingly, the MC3T3-E1/4B12 co-cultures with nHAp/IO@miR-21/124 maintained under the magnetic field were characterized by slightly lower RUNX-2 expression; however, it was still increased when compared to the control (Figure 5A). Modulatory effect of nHAp/IO@miR-21/124 and magnetic field toward MC3T3-E1/4B12 was also evidenced in relation to the osteopontin (OPN) expression (Figure 7). The functionalised biomaterial strongly increased OPN transcripts levels in cultures propagated without magnetic field exposure. Surprisingly, MC3T3-E1/4B12 cells cultured with nHAp/IO@miR-21/124 nanocomposite in the presence of magnetic field were characterised by a lower expression of OPN (Figure 8).

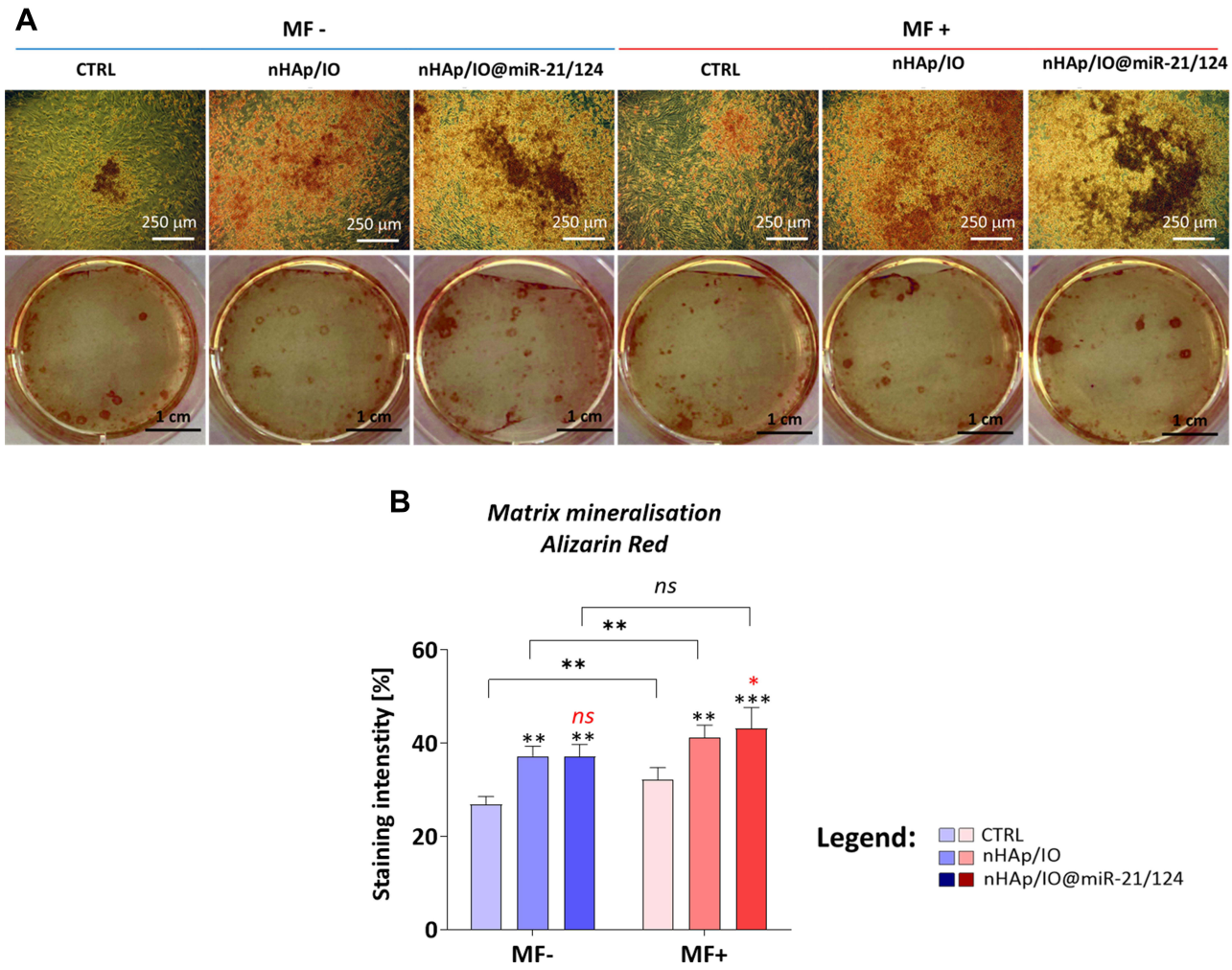

Figure 2 Nanocomposite nHAp/IO@miR-21/124 enhances osteogenic differentiation in MC3T3-E1/4B12 co-cultures. (**A**) Representative pictures of osteogenic nodules formed during the differentiation. Scale bars indicated in the photographs. (**B**) Comparison of Alizarin Red staining intensity. Obtained data were used for comparative analysis and presented as columns with bars representing means ± SD. Marks: * $p<0.05$; ** $p < 0.01$; *** $p<0.001$ and non-significant differences were indicated using ns symbol. The differences between nHAp/IO and nHAp/IO@miR-21/124 were marked with red font.

Modulatory Effect of the Scaffold on Bone-Related Transcripts (miRNA Level)

The late differentiation of osteoblast in cultures with nHAp/IO@miR-21/124 was also explicitly evidenced based on miRNA levels (Figure 4). We have shown that miRNA molecules that play a pivotal role as inhibitors of osteoblastic differentiation are downregulated in cultures treated with functionalised nanocomposite, ie nHAp/IO@miR-21/124. We noted lowered levels of miR-7a-5p, miR-17-5p, miR-223-3p and miR-320a-3p, both under and without magnetic field influence (Figure 4C-F). The analysis of miR-21 and miR-124 levels confirms the potential regulatory effect of nHAp/IO@miR-21/124 on the transcript levels. The cells responded on nHAp/IO@miR-21/124 with increased expression of miR-21, both in cultures without and under magnetic field activity (Figure 4A). In turn, the miR-124 levels were elevated only in cultures without exposition to the magnetic field (Figure 4B).

The Scaffolds Modulate the Protein Expression of runt-Related Transcription Factor 2 (RUNX-2) and Osteopontin (OPN)

Western blot analysis revealed increased expression of RUNX-2 protein in response to the nanocomposite functionalised with miR-21/124 complex, only in cultures maintained without magnetic field exposure. In turn, lowered accumulation of RUNX-2 was noted in cultures propagated with nanocomposites exposed to the magnetic field (Figure 5B–D). However, immunofluorescent

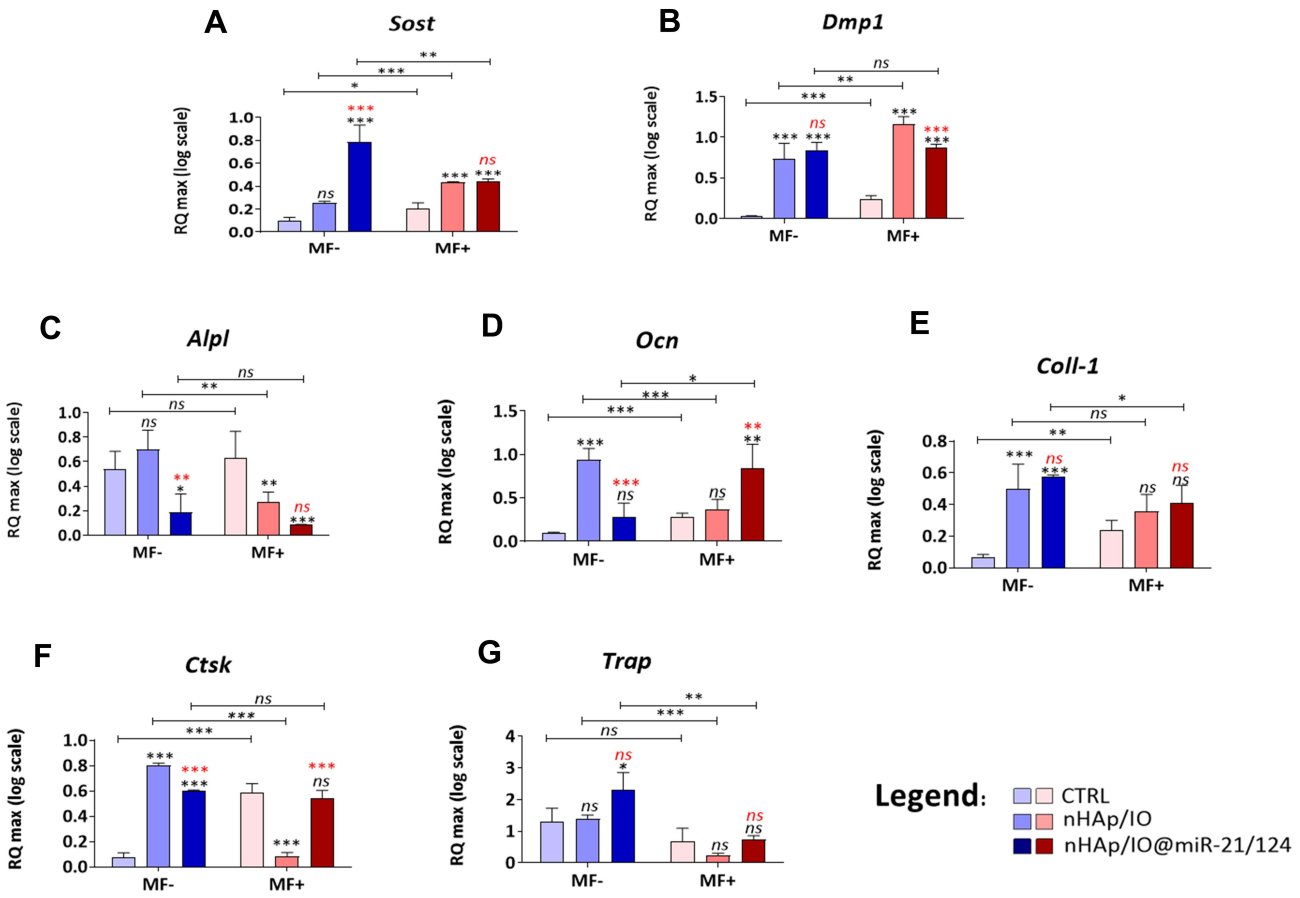

Figure 3 Nanocomposite nHAp/IO@miR-21/124 modulates the mRNA expression for pro-osteogenic transcripts inducing osteocyte-like phenotype characteristic in mineralised tissue. RT-PCR analysis of (**A**) sclerostin (Sost), (**B**) dentin matrix protein 1 (Dmp1). (**C**) alkaline phosphate (*Alp*). (**D**) osteocalcin (*Ocn*). (**E**) collagen type I (Coll-I). (**F**) cathepsin (**K**) (Ctsk). (**G**) Tartrate-resistant acid phosphatase (*Trap*). Relative quantification was performed in reference to the sample with the lowest expression of the target gene (RQmax) after normalisation to glyceraldehyde 3-phosphate dehydrogenase (*Gapdh*). Normalised values are presented as columns with bars representing means ± SD. Marks: *p<0.05; **p < 0.01; ***p<0.001 and non-significant differences were indicated using ns symbol. The differences between nHAp/IO and nHAp/IO@miR-21/124 were marked with red font.

visualization of RUNX-2 deposits confirmed its increased accumulation driven by nHAp/IO@miR-21/124 and magnetic field exposure (Figure 6).

Modulatory effect of nHAp/IO@miR-21/124 and magnetic field toward MC3T3-E1/4B12 was also evidenced in relation to the osteopontin (OPN) expression (Figure 7). The functionalised biomaterial significantly increased protein levels in cultures propagated without magnetic field exposure. In turn, osteogenic cultures affected by nHAp/IO@miR-21/124 and magnetic field exposure were characterised by lowered expression of OPN measured at the protein level, with reference to the control conditions. Nevertheless, the OPN intracellular localisation analysis confirmed increased expression of OPN guided by the biomaterial without magnetic influence (Figure 8). However, immunocytochemistry staining also revealed that OPN expression decreases under the magnetic field. Yet, the OPN expression in cultures with nanocomposites remained increased when compared to the control cultures. Obtained results are consistent with the late-osteoblast phenotype of differentiated osteoblasts.

The Assessment of Scaffold Utility in a Model of Senile Osteoporosis

The in vivo study performed on the senescence senile-osteoporosis model, ie SAM/P6 mice, confirmed the pro-osteogenic effect of nHAp/IO@miR-21/124 composite without magnetic field exposure (Figure 9). The biomaterial promoted new bone formation in mice with lowered bone metabolism (SAM/P6). Additionally, a complete internalization of biomaterial with bone tissue of Balb/3T3 mice was observed – after 6 weeks after implantation. The scaffold was replaced by functional tissue. Both in SAM/P6 and Babl/3T3 mice, the biomaterial improved bone density and quality reflected by increased bone volume per total volume

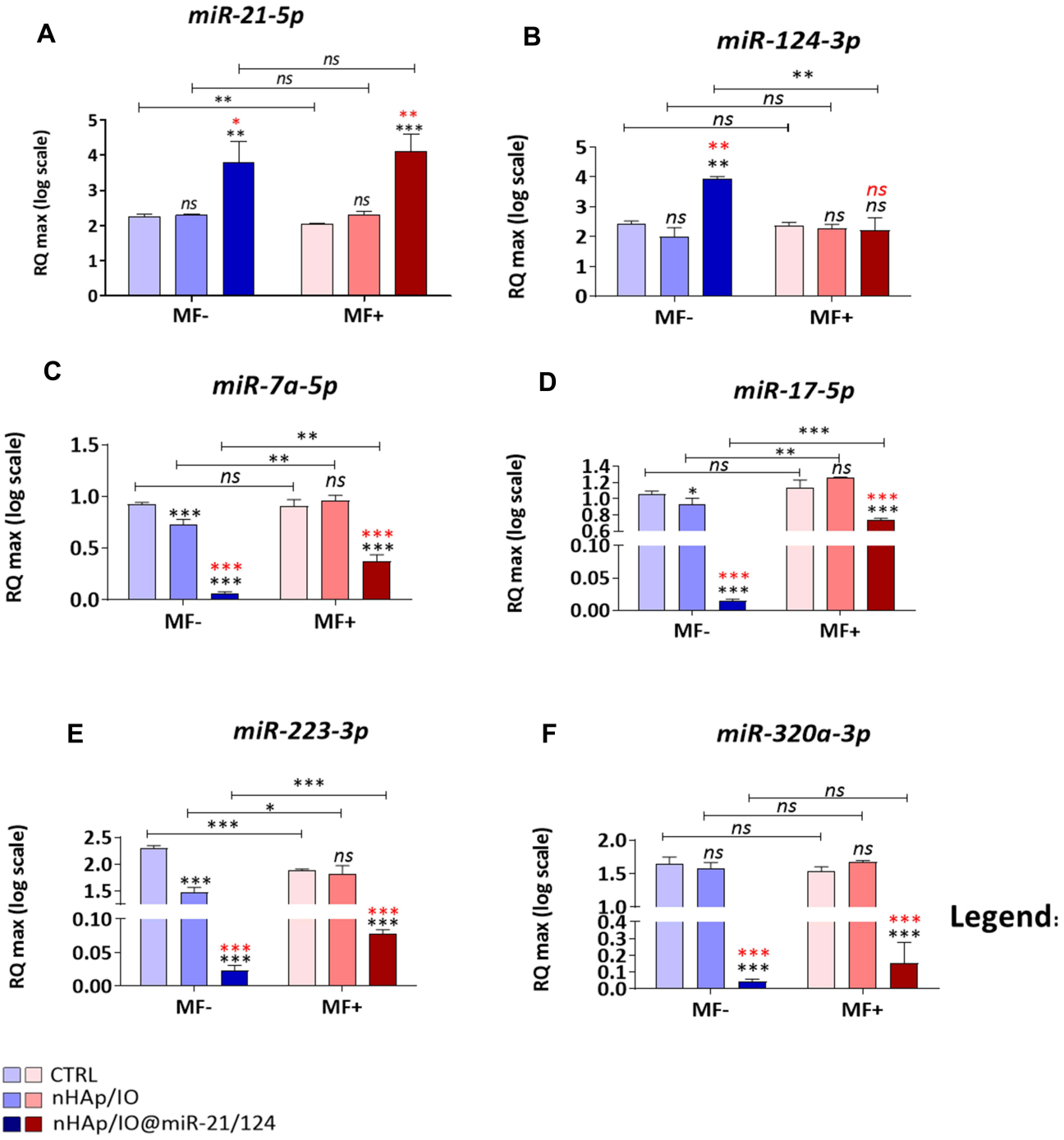

Figure 4 Nanocomposite nHAp/IO@miR-21/124 regulates expression of small non-coding RNA (miRNA) involved in osteogenic differentiation. RT-PCR analysis of (**A**) miR-21-5p. (**B**) miR-124-3p. (**C**) miR-7a-5p. (**D**) miR-17-5p. (**E**) miR-223-3p and (**F**) miR-320a-3p. Relative quantification of miRNA levels was made regarding to the sample with the lowest expression of the miRNA transcripts (RQmax) after normalisation to non-coding small nuclear RNA (*snU6*). Normalised values are presented as columns with bars representing means ± SD. Marks: *p<0.05; **p < 0.01; ***p<0.001 and non-significant differences were indicated using ns symbol. The differences between nHAp/IO and nHAp/IO@miR-21/124 were marked with red font.

ratio (BV/TV) (Figure 9D). The obtained results are consistent with in vitro assays, showing enhanced mineralization of the extracellular bone matrix produced by differentiated osteoblasts, which is guided by the nanocomposite biological activity.

Discussion

In the presented study, we have shown that obtained nHAp/IO@miR21/124 scaffold presented pro-osteogenic activity in the MC3T3-E1/4B12 co-cultures and promoted new bone formation in the SAM/P6 osteoporotic mice

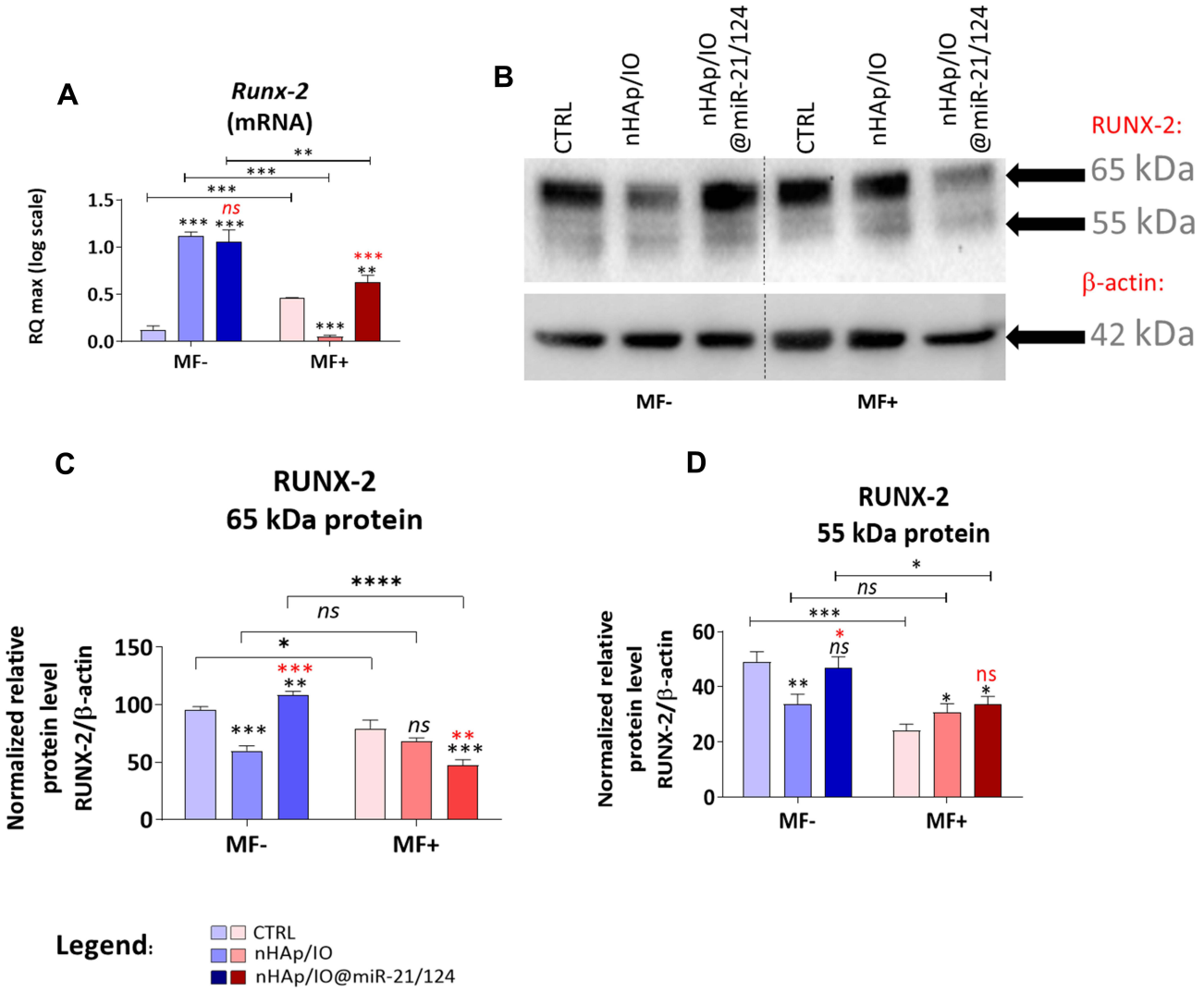

Figure 5 The expression of runt-related transcription factor (Runx-2) is modulated by nanocomposites and exposition to the magnetic field. (**A**) Quantification of Runx-2 transcripts determined using RT-qPCR. (**B**) Representative blots showing the intracellular accumulation of RUNX-2 and reference protein, ie β-actin. (**C**) Results of densitometric measurement of protein expression, performed for bands corresponding with 65kDA RUNX-2. (**D**) Results of densitometric measurement of protein expression, performed for bands corresponding with 55kDA RUNX-2. Normalised values are presented as columns with bars representing means ± SD. Marks: *p<0.05; **p < 0.01; ***p<0.001 and non-significant differences were indicated using ns symbol. The differences between nHAp/IO and nHAp/IO@miR-21/124 were marked with red font.

model. We have observed intensified formation of mineralized extracellular matrix and increased expression of late osteogenesis markers including sclerostin (Sost), dentin matrix protein 1 (Dmp1), collagen type 1(Coll-1), osteocalcin (Ocn) and miR-21 in the MC3T3-E1/4B12 co-cultures. Importantly, it has been previously demonstrated that not only does miR-21 target expression of Coll-1 and Ocn[32] but it also plays a crucial role in regulating osteogenic differentiation of MC3T3 pre-osteoblasts and osteoblasts-osteoclast coupling[7] Our previous studies showed that miRNA-21 regulates the expression of a master transcription factor, critical for osteoblasts differentiation, ie Runx-2, as well as osteopontin, which is extracellular matrix protein with a dual role, essential for bone mineralization and survival of osteoclasts.[7]

The obtained results confirmed that nHAp/IO@miR-21/124 nanocomposite promotes molecular phenotype alteration, typical for pre-osteocytes and/or osteocytes, associated with mineralized, calcium-rich ECM. Additionally, we also demonstrated that nHAp/IO@miR-21/124 nanocomposite decreased levels of miRNA that negatively regulate the process of bone-forming cells differentiation such as miR-7a-5p, miR-17-5p, miR-223-3p and miR-320a-3p.[33–36] Thus, we conclude that the obtained composites play an essential role as a platform mediating osteogenesis via mRNA-miRNA axis, which

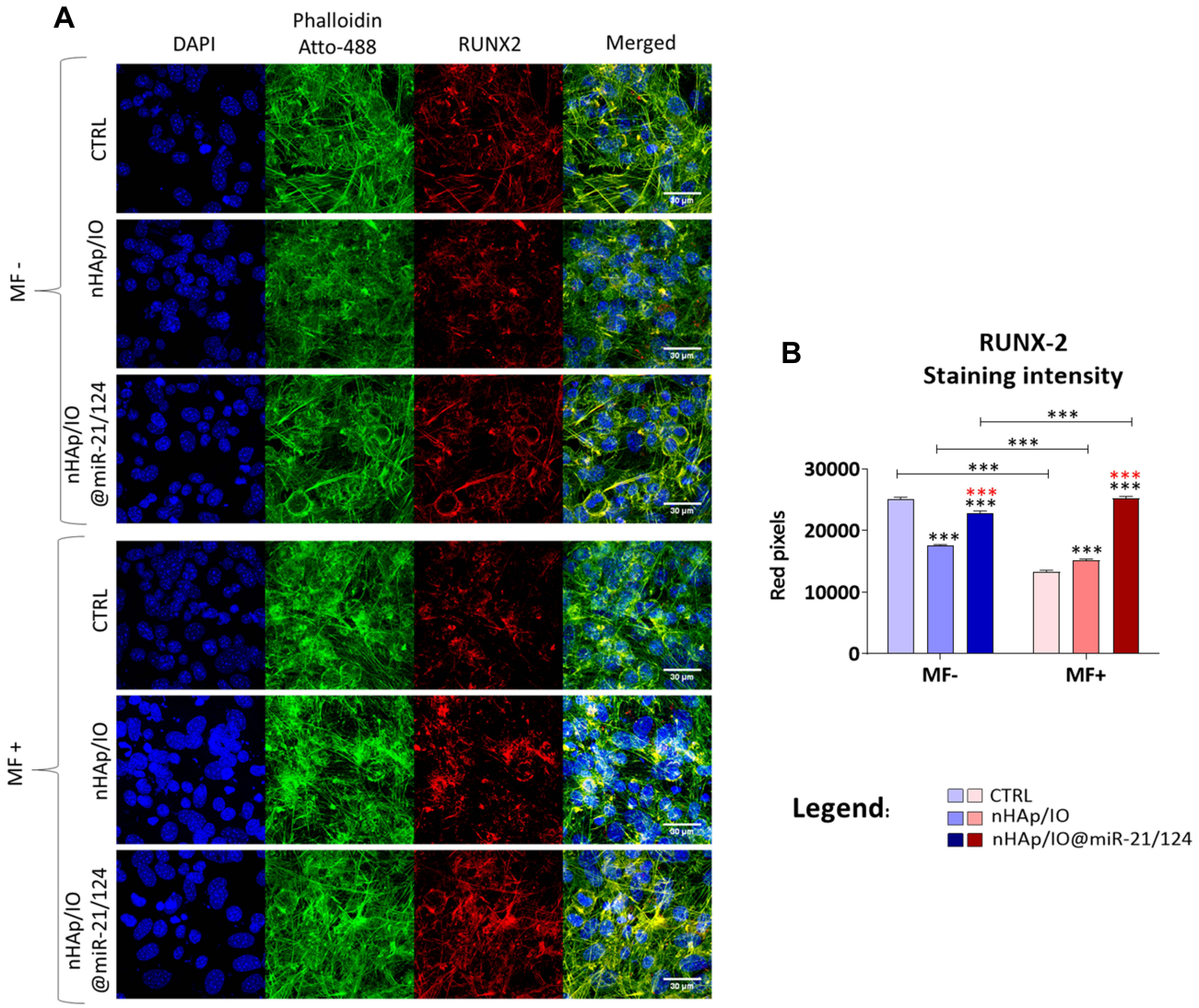

Figure 6 The intracellular distribution of RUNX-2. (**A**) Representative microphotographs obtained by confocal imaging, showing colocalization of RUNX-2 with nuclei (DAPI, blue-stained) and actin cytoskeleton (phalloidin Atto-488, green-stained). (**B**) Results of signal intensity analysis performed to compare the influence of experimental conditions on RUNX-2 expression. Obtained values are presented as columns with bars representing means ± SD. Marks: ***p<0.001. The differences between nHAp/IO and nHAp/IO@miR-21/124 were marked with red font.

results in an accelerated differentiation process of osteoblasts precursors. As osteoporotic bone regeneration requires targeting the osteoclast activity, miR-124 has also been proposed to be a critical agent that modulates its metabolic activity and function.[22] Numerous studies, including our previous findings, showed that enhanced expression of miR-124 strongly correlated with osteoclasts activity.[22,23,27] Recently, Tang and colleagues showed that miR-124 decreases osteogenic differentiation of bone marrow-derived mesenchymal stem cells (BM-MSCs), the Sp7 molecule was proposed as a potential target of miR-124.[23] Given the contradictions regarding the molecular role of miR-124 during bone regeneration, we aimed to verify our hypothesis if local delivery of miR-124 together with miR-21 might become a potential therapeutic solution for osteoporotic bone regeneration and the obtained results strongly indicate a positive effect of the proposed miRNA combination.

The in vitro study confirmed the cytocompatibility of nHAp/IO and indicated the anti-apoptotic activity of the scaffolds, regardless of magnetic field influence. Interestingly, we observed that an external static magnetic field was not a critical factor for promoting signaling essential for osteoblast development. Notably, the magnetic field influence resulted in reduced RNA expression for tartrate-resistant acid phosphatase (TRAP), a marker of

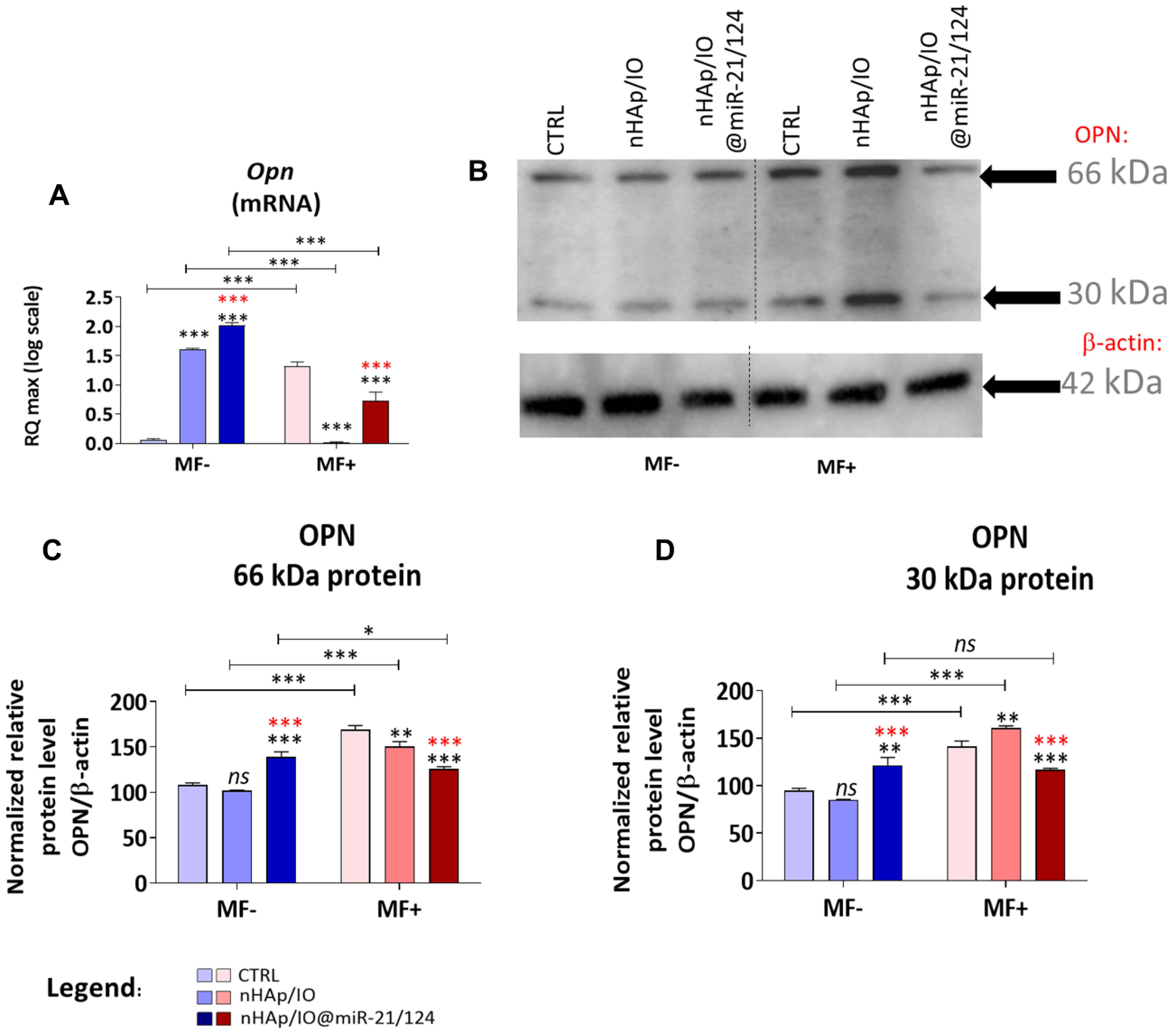

Figure 7 The expression of osteopontin (OPN) is regulated by nanocomposites and exposition to the magnetic field. (**A**) Determination of mRNA levels for *Opn* using RT-qPCR. (**B**) Representative blots showing the intracellular accumulation of OPN with reference to β-actin (ACTB) expression. (**C**) Results of densitometric measurement of protein expression, performed for bands corresponding with 66kDA OPN. (**D**) Results of densitometric measurement of protein expression, performed for bands corresponding with 30kDA OPN. Normalised values are presented as columns with bars representing means ± SD. Marks: *p<0.05; **p < 0.01; ***p<0.001 and non-significant differences were indicated using ns symbol. The differences between nHAp/IO and nHAp/IO@miR-21/124 were marked with red font.

active bone-resorbing osteoblasts. This observation is in good agreement with the study of Pi et al, who showed that osteoclastogenesis decreased after the exposition of murine monocyte-macrophage lineage (RAW 264.7) to the low-frequency pulsed electromagnetic field and was associated with the lowered activity of TRAP.[37]

In order to test the pro-osteogenic effectiveness of the scaffolds, we performed a bilateral cranial defect model in senescence-accelerated mouse prone 6 (SAM/P6) and evaluated the process of bone healing. Since SAM/P6 represents the model of senile osteoporosis with low bone mass and reduced bone mineral density, verification of clinical effectiveness using this model is fully justified. In this study, we have observed that transplanted nHAp/IO@miR-21/124 improved bone regeneration after 6 weeks post-operation as well as promoted new bone formation as compared to the control group, as visualized by micro-CT analysis. The obtained results are in line with previous findings of Sun et al, who showed that miR-21 nanocapsules promote early bone repair of osteoporotic fractures in ovariectomised rats by stimulating the osteogenic differentiation of bone marrow mesenchymal stem cells.[21] Moreover, Yang et al demonstrated that miRNA-21 enhanced bone regeneration in critical-size defects and

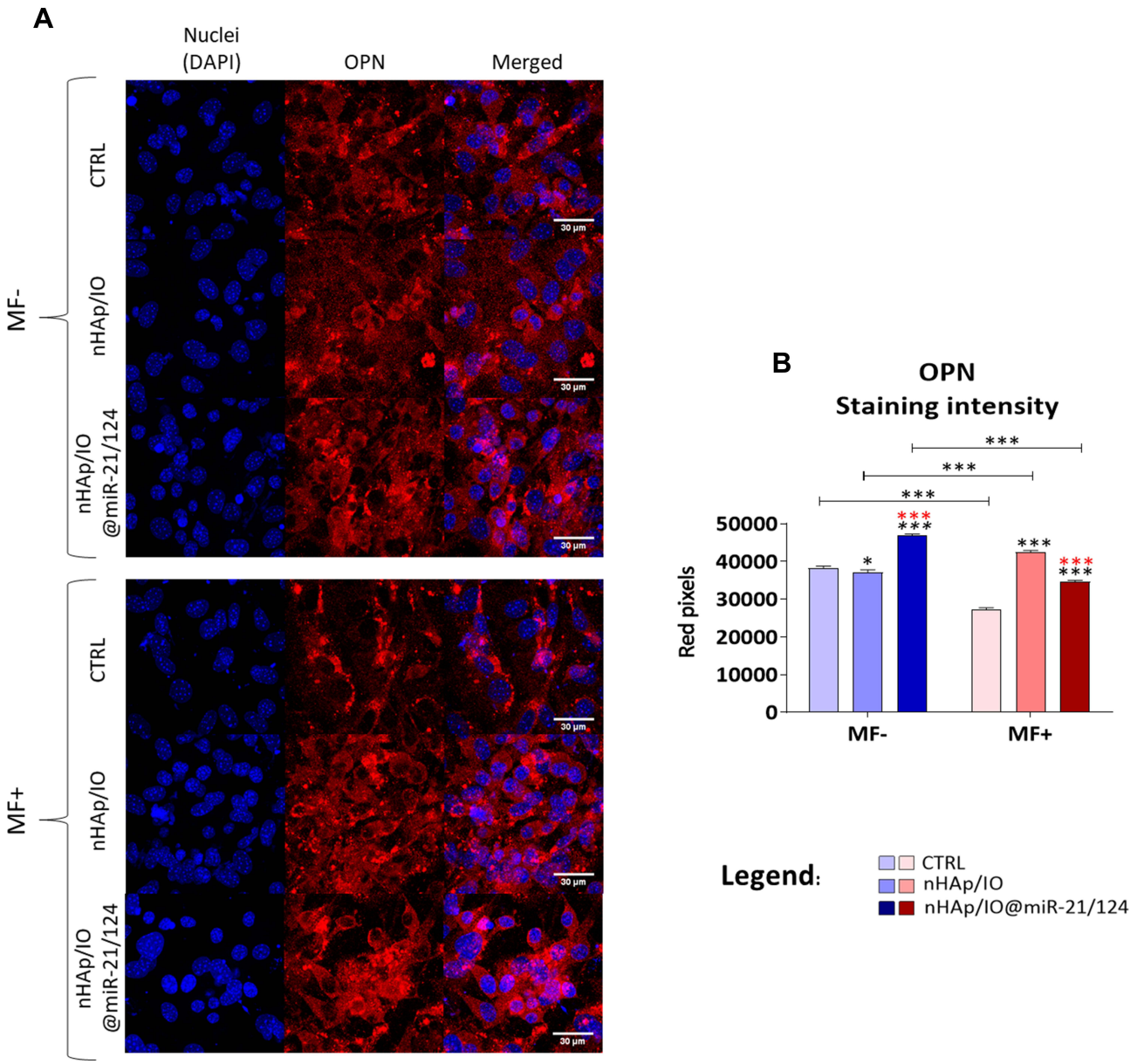

Figure 8 The intracellular distribution of osteopontin (OPN) determined using immunocytochemistry. (**A**) Representative microphotographs obtained by confocal imaging, showing colocalization of OPN with nuclei (DAPI, blue-stained). (**B**) Results of signal intensity analysis performed to compare the influence of experimental conditions on OPN expression. Obtained values are presented as columns with bars representing means ± SD. Marks: *p<0.05 and ***p<0.001. The differences between nHAp/IO and nHAp/IO@miR-21/124 were marked with red font.

promoted differentiation of osteoblast recruited from bone marrow progenitors by PTEN/PI3K/Akt/HIF-1α signals.[38]

Importantly, the small sample size (BALBc n=2, SAM/P6 n=2) planned for the in vivo model is the main limitation of the study. The model was implemented in order to further confirm the in vitro findings on a senile osteoporotic model represented by SAM/P6 mice. Based on the obtained results, an additional experiment has been planned with a more complex approach to verify the therapeutic potential of the developed nHAp/IO@miR-21/124 platform.

In summary, we conclude that the pro-osteogenic effect of the developed nHAp/IO@miR-21/124 scaffolds may be associated with ameliorated differentiation of osteoblast precursors, osteoblast-to-osteocyte transformation and activation of signals reducing the activity of osteoclasts.

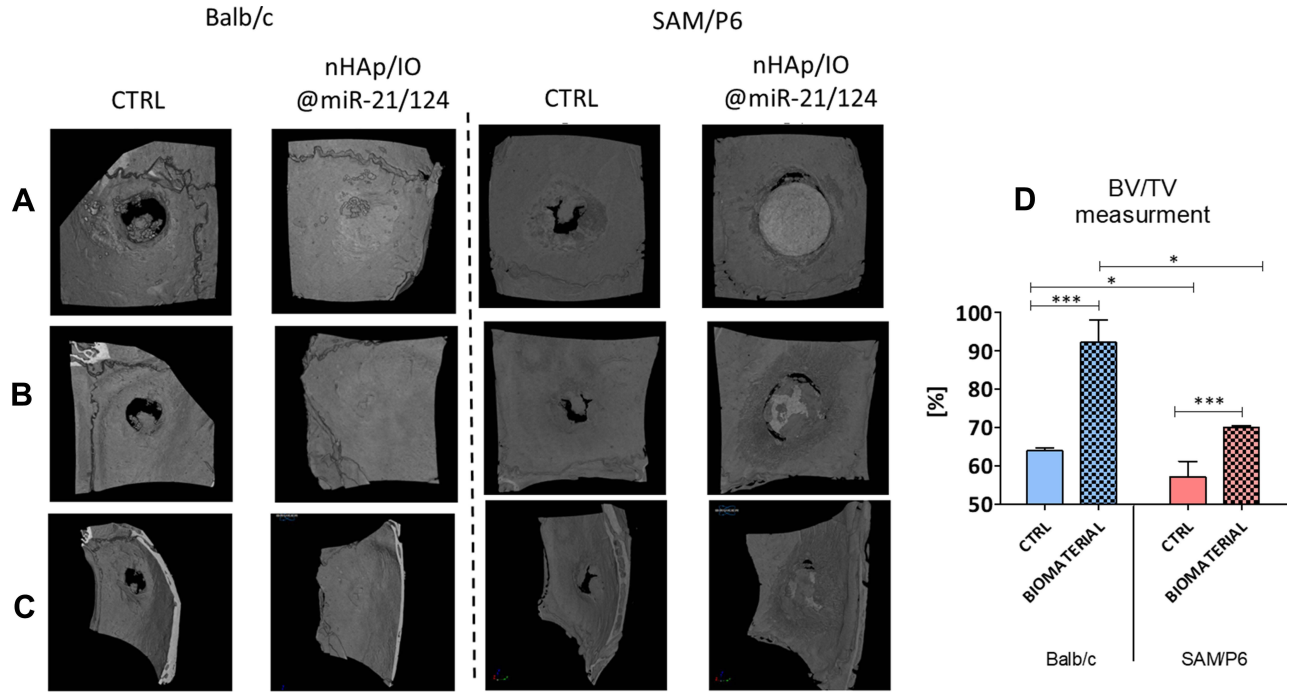

Figure 9 Nanocomposite, nHAp/IO@miR-21/124 increase bone density in vivo. MicroCT reconstructions of the burr holes in the control defect (CTRL) and the burr holes with the nanocomposite (nHAp/IO@miR-21/124). (**A**) Top surface of the cranial bone. (**B**) Bottom view of the regenerated bone. (**C**) Side picture of the regenerated cranial bone. (**D**) Results of comparative analysis of bone volume per total volume ratio (BV/TV) in the repaired cranial defect area of the animals, ie mice Balb/c stain and osteoporotic model, ie SAM/P6 mice. Marks: *p<0.05; and ***p<0.001.

Conclusion

We showed that nHAp/IO might serve as an efficient delivery system for therapeutic miRNAs, ie miR-21 and miR-124. Developed nHAp/IO@miR-21/124 scaffold presents pro-osteogenic activity regulating proper coupling of osteoblast and osteoclast at a post-transcriptional level in osteoporotic conditions. This study sheds promising light on the potential usefulness of nHAp/IO@miR-21/124 platform as an auto-associative system promoting the formation of fully functional bone in a model of senile osteoporosis (ie, SAM/P6 mice). The obtained therapeutic platform may find application in nanomedicine, especially as a factor promoting the healing of deteriorated bone tissue, including osteoporotic bone.

Acknowledgments

Financial support from the National Science Centre over the course of the realisation of the project Harmonia 10 titled New, two-stage scaffolds based on calcium nanoapatite (nHAP) incorporated with iron nanotoxides (Fe_2O_3/Fe_3O_4) as a function of controlled release of miRNA in a static magnetic field for the regeneration of bone fractures in osteoporotic patients (Grant No. UMO 2017/26/M/NZ5/01184) is gratefully acknowledged. The publication is financed under the Leading Research Groups support project from the subsidy increased for the period 2020–2025 in the amount of 2% of the subsidy referred to Art. 387 (3) of the Law of 20 July 2018 on Higher Education and Science, obtained in 2019. We also thank Klaudia Marcinkowska and Mateusz Sikora for their help during in vitro studies and Professor Zbigniew J. Król for consultation of microCT results during the revision process. We would like thank to M.Sc. Adrian Patej for helping during physicochemical characterisation of biomaterials.

Disclosure

The authors report no conflicts of interest in this work.

References

1. Sözen T, Özışık L, Başaran NÇ. An overview and management of osteoporosis. *Eur J Rheumatol*. 2017;4:46–56. doi:10.5152/eurjrheum.2016.048
2. Tobias JH, Duncan EL, Kague E, et al. Opportunities and Challenges in functional genomics research in osteoporosis: report from a Workshop Held by the Causes Working Group of the Osteoporosis and Bone Research Academy of the Royal Osteoporosis Society on October 5th 2020. *Front Endocrinol*. 2021;11. doi:10.3389/fendo.2020.630875
3. Eskandarynasab M, Etemad-Moghadam S, Alaeddini M, et al. Novel osteoprotective nanocochleate formulation: a dual combination therapy-codelivery system against glucocorticoid induced osteoporosis. *Nanomedicine*. 2020;29:102273. doi:10.1016/j.nano.2020.102273

4. Zhao R, Chen S, Zhao W, et al. A bioceramic scaffold composed of strontium-doped three-dimensional hydroxyapatite whiskers for enhanced bone regeneration in osteoporotic defects. *Theranostics*. 2020;10:1572–1589. doi:10.7150/thno.40103
5. Bai H, Zhao Y, Wang C, et al. Enhanced osseointegration of three-dimensional supramolecular bioactive interface through osteoporotic microenvironment regulation. *Theranostics*. 2020;10(11):4779–4794. doi:10.7150/thno.43736
6. Noh J-Y, Yang Y, Jung H. Molecular mechanisms and emerging therapeutics for osteoporosis. *Int J Mol Sci*. 2020;21(20):7623. doi:10.3390/ijms21207623
7. Smieszek A, Marcinkowska K, Pielok A, et al. The role of miR-21 in osteoblasts–osteoclasts coupling in vitro. *Cells*. 2020;9(2):479. doi:10.3390/cells9020479
8. Tencerova M, Kassem M. The bone marrow-derived stromal cells: commitment and regulation of adipogenesis. *Front Endocrinol*. 2016;7. doi:10.3389/fendo.2016.00127
9. Macías I, Alcorta-Sevillano N, Rodríguez CI, Infante A. Osteoporosis and the potential of cell-based therapeutic strategies. *Int J Mol Sci*. 2020;21(5):1653. doi:10.3390/ijms21051653
10. Tang Q, Hu Z, Jin H, et al. Microporous polysaccharide multilayer coated BCP composite scaffolds with immobilised calcitriol promote osteoporotic bone regeneration both in vitro and in vivo. *Theranostics*. 2019;9:1125–1143. doi:10.7150/thno.29566
11. Weivoda MM, Chew CK, Monroe DG, et al. Identification of osteoclast-osteoblast coupling factors in humans reveals links between bone and energy metabolism. *Nat Commun*. 2020;11(87). doi:10.1038/s41467-019-14003-6.
12. Yang Y-S, Xie J, Chaugule S, et al. Bone-targeting AAV-mediated gene silencing in osteoclasts for osteoporosis therapy. *Mol Ther*. 2020;17:922–935. doi:10.1016/j.omtm.2020.04.010
13. Sterling JA, Guelcher SA. Biomaterial scaffolds for treating osteoporotic bone. *Current Osteoporosis Reports*. 2014;12(1):48–54. doi:10.1007/s11914-014-0187-2
14. Salamanna F, Gambardella A, Contartese D, Visani A, Fini M. Nano-based biomaterials as drug delivery systems against osteoporosis: a systematic review of preclinical and clinical evidence. *Nanomaterials (Basel)*. 2021;11(2):530. doi:10.3390/nano11020530
15. Codrea CI, Croitoru A-M, Baciu CC, et al. Advances in osteoporotic bone tissue engineering. *J Clin Med*. 2021;10(2):253. doi:10.3390/jcm10020253
16. Bayani M, Torabi S, Shahnaz A, Pourali M. Main properties of nanocrystalline hydroxyapatite as a bone graft material in treatment of periodontal defects. A review of literature. *Biotechnol Biotechnol Equip*. 2017;31(2):215–220. doi:10.1080/13102818.2017.1281760
17. Lowe B, Hardy JG, Walsh LJ. Optimizing nanohydroxyapatite nanocomposites for bone tissue engineering. *ACS Omega*. 2019;5:1–9. doi:10.1021/acsomega.9b02917
18. Marycz K, Sobierajska P, Roecken M, et al. Iron oxides nanoparticles (IOs) exposed to magnetic field promote expression of osteogenic markers in osteoblasts through integrin alpha-3 (INTa-3) activation, inhibits osteoclasts activity and exerts anti-inflammatory action. *J Nanobiotechnology*. 2020;18(1):33. doi:10.1186/s12951-020-00590-w
19. Sikora M, Marycz K, Smieszek A. Small and long non-coding RNAs as functional regulators of bone homeostasis, acting alone or cooperatively. *Mol Ther Nucleic Acids*. 2020;21:792–803. doi:10.1016/j.omtn.2020.07.017
20. Wei F, Yang S, Guo Q, et al. MicroRNA-21 regulates osteogenic differentiation of periodontal ligament stem cells by targeting Smad5. *Sci Rep*. 2017;7:16608. doi:10.1038/s41598-017-16720-8
21. Sun X, Li X, Qi H, et al. MiR-21 nanocapsules promote early bone repair of osteoporotic fractures by stimulating the osteogenic differentiation of bone marrow mesenchymal stem cells. *J Orthop Translat*. 2020;24:76–87. doi:10.1016/j.jot.2020.04.007
22. Lee Y, Kim HJ, Park CK, et al. MicroRNA-124 regulates osteoclast differentiation. *Bone*. 2013;56:383–389. doi:10.1016/j.bone.2013.07.007
23. Tang J-Z, Lin X, Zhong JY, et al. miR-124 regulates the osteogenic differentiation of bone marrow-derived mesenchymal stem cells by targeting Sp7. *Mol Med Rep*. 2019;19:3807–3814.
24. Amano S, Sekine K, Bonewald LF, Ohmori Y. A novel osteoclast precursor cell line, 4B12, recapitulates the features of primary osteoclast differentiation and function: enhanced transfection efficiency before and after differentiation. *J Cell Physiol*. 2009;221:40–53. doi:10.1002/jcp.21827
25. Seweryn A, Pielok A, Lawniczak-Jablonska K, et al. Zirconium oxide thin films obtained by atomic layer deposition technology abolish the anti-osteogenic effect resulting from miR-21 inhibition in the pre-osteoblastic MC3T3 cell line. *Int J Nanomedicine*. 2020;15:1595–1610. doi:10.2147/IJN.S237898
26. Smieszek A, Seweryn A, Marcinkowska K, et al. Titanium dioxide thin films obtained by atomic layer deposition promotes osteoblasts' viability and differentiation potential while inhibiting osteoclast activity-potential application for osteoporotic bone regeneration. *Materials (Basel)*. 2020;13(21):4817. doi:10.3390/ma13214817
27. Marycz K, Smieszek A, Marcinkowska K, et al. Nanohydroxyapatite (nHAp) doped with iron oxide nanoparticles (IO), miR-21 and miR-124 under magnetic field conditions modulates osteoblast viability, reduces inflammation and inhibits the growth of osteoclast – a novel concept for osteoporosis treatment: Part 1. *Int J Nanomedicine*. 2021;16:3429–3456.
28. Śmieszek A, Stręk Z, Kornicka K, et al. Antioxidant and anti-senescence effect of metformin on mouse olfactory ensheathing cells (mOECs) may be associated with increased brain-derived neurotrophic factor levels-an ex vivo study. *Int J Mol Sci*. 2017;18(4):872. doi:10.3390/ijms18040872
29. Marycz K, Weiss C, Śmieszek A, Kornicka K. Evaluation of oxidative stress and mitophagy during adipogenic differentiation of adipose-derived stem cells isolated from Equine Metabolic Syndrome (EMS) horses. *Stem Cells Int*. 2018;2018. doi:10.1155/2018/5340756
30. Smieszek A, Kornicka K, Szłapka-Kosarzewska J, et al. Metformin increases proliferative activity and viability of multipotent stromal stem cells isolated from adipose tissue derived from horses with equine metabolic syndrome. *Cells*. 2019;8(2):80. doi:10.3390/cells8020080
31. Smieszek A, Tomaszewski KA, Kornicka K, Marycz K. Metformin promotes osteogenic differentiation of adipose-derived stromal cells and exerts pro-osteogenic effect stimulating bone regeneration. *J Clin Med*. 2018;7(12):482. doi:10.3390/jcm7120482
32. Li H, Yang F, Wang Z, Fu Q, Liang A. MicroRNA-21 promotes osteogenic differentiation by targeting small mothers against decapentaplegic 7. *Mol Med Rep*. 2015;12:1561–1567. doi:10.3892/mmr.2015.3497
33. Li X, Zheng Y, Zheng Y, et al. Circular RNA CDR1as regulates osteoblastic differentiation of periodontal ligament stem cells via the miR-7/GDF5/SMAD and p38 MAPK signaling pathway. *Stem Cell Res Ther*. 2018;9(232). doi:10.1186/s13287-018-0976-0.
34. Chen N, Wu D, Li H, Liu Y, Yang H. MiR-17-3p inhibits osteoblast differentiation by downregulating Sox6 expression. *FEBS Open Bio*. 2020;10:2499–2506. doi:10.1002/2211-5463.12979
35. Zhang S, Liu Y, Zheng Z, et al. MicroRNA-223 suppresses osteoblast differentiation by inhibiting DHRS3. *CPB*. 2018;47:667–679.
36. Huang J, Meng Y, Liu Y, et al. MicroRNA-320a regulates the osteogenic differentiation of human bone marrow-derived mesenchymal stem cells by targeting HOXA10. *CPB*. 2016;38:40–48.
37. Pi Y, Liang H, Yu Q, et al. Low-frequency pulsed electromagnetic field inhibits RANKL-induced osteoclastic differentiation in RAW264.7 cells by scavenging reactive oxygen species. *Mol Med Rep*. 2019;19:4129–4136.
38. Yang C, Liu X, Zhao K, et al. miRNA-21 promotes osteogenesis via the PTEN/PI3K/Akt/HIF-1α pathway and enhances bone regeneration in critical size defects. *Stem Cell Res Ther*. 2019;10(65). doi:10.1186/s13287-019-1168-2.